

Article

Self-Luminous Wood Coatings with Carbon Dots/TiO₂ Grafted Afterglow SrAl₂O₄: Eu, Dy Core-Shell Phosphors for Long-Lasting Formaldehyde Removal

Longfei Zhang ^{1,2,3}, Ying Wang ¹, Limin Peng ¹, Zhilin Chen ¹ , Shaoyi Lyu ^{1,2,3,*} and Siqun Wang ^{4,*} 

¹ Research Institute of Wood Industry, Chinese Academy of Forestry, Beijing 100091, China; zhanglongfei@caf.ac.cn (L.Z.)

² Co-Innovation Center of Efficient Processing and Utilization of Forest Resources, Nanjing Forestry University, Nanjing 210037, China

³ National Forestry and Grassland Administration Key Laboratory of Plant Fiber Functional Materials, Fuzhou 350002, China

⁴ Center for Renewable Carbon, University of Tennessee, Knoxville, TN 37996, USA

* Correspondence: lvsy@caf.ac.cn (S.L.); swang@utk.edu (S.W.)

Abstract: Long-term relief of indoor volatile pollution has become a competitive issue worldwide in both visible and dark environments. A novel self-luminous wood coating with carbon dots (CDs)/titanium dioxide (TiO₂) nanomaterial coated SrAl₂O₄: Eu²⁺, Dy³⁺ (CDs/TiO₂@SAO) composite was prepared for the long-term degradation of formaldehyde through a simple sol-gel method. The microstructure, chemical composition, ultraviolet-visible (UV-vis) spectra, and long-lasting fluorescence of the CDs/TiO₂@SAO photocatalyst were analyzed to illustrate the mechanism for degrading formaldehyde. The obtained CDs with a particle size of ~2–7 nm have a good graphite structure and presented good absorption in visible light. In addition, owing to the synergistic effect of the CDs/TiO₂ nanomaterial coating layer and the long-afterglow luminescence of the SAO phosphor, the CDs/TiO₂@SAO composite can absorb a part of the visible light for photocatalytic degradation and store luminous energy efficiently at daytime so as to give out visible luminescence continuously for a few hours in the darkness. Furthermore, the functional wood coatings with CDs/TiO₂@SAO composite presented continuous and efficient photocatalytic activity in the presence and absence of light exposure. The current research could provide a new strategy for designing an efficient photocatalyst for degrading formaldehyde pollution in the daytime with a visible light supply and in an indoor dark environment without an external light source.

Keywords: carbon dots; core-shell microspheres; SrAl₂O₄: Eu²⁺, Dy³⁺ phosphor; titanium dioxide; surface modification; photocatalytic degradation



Citation: Zhang, L.; Wang, Y.; Peng, L.; Chen, Z.; Lyu, S.; Wang, S. Self-Luminous Wood Coatings with Carbon Dots/TiO₂ Grafted Afterglow SrAl₂O₄: Eu, Dy Core-Shell Phosphors for Long-Lasting Formaldehyde Removal. *Polymers* **2023**, *15*, 2077. <https://doi.org/10.3390/polym15092077>

Academic Editor: Hiroshi Yoshihara

Received: 10 March 2023

Revised: 14 April 2023

Accepted: 26 April 2023

Published: 27 April 2023



Copyright: © 2023 by the authors. Licensee MDPI, Basel, Switzerland. This article is an open access article distributed under the terms and conditions of the Creative Commons Attribution (CC BY) license (<https://creativecommons.org/licenses/by/4.0/>).

1. Introduction

Recently, indoor volatile organic pollutants (VOCs) have attracted more attention from researchers [1–3]. It is well known that construction materials and indoor decorations such as paintings, wallpapers, textiles, and wood functional panels generally release formaldehyde and other organic volatiles [4,5]. Among these indoor organic pollutants, the formaldehyde hazardous volatile pollutant is regarded as a typical air pollution owing to its potential threat to human health. Generally, the highest allowable concentration of formaldehyde in indoor air should be limited to less than 0.08 mg/m³ [6,7]. People in the living environment will have an obvious discomfort in mentality and physiology once the formaldehyde concentration reaches more than 0.10 mg/m³. Numerous studies have indicated that long-term exposure to the atmosphere containing a high concentration of formaldehyde could induce respiratory diseases, chronic poisoning, and even death [8,9]. Therefore, it is of great significance to develop novel approaches and materials for removing formaldehyde from our living environment.

Among the technologies developed for the treatment of organic pollutants, the regular strategies include plant purification, activated carbon adsorption, photocatalysis, and high-energy plasma treatment [10–12]. In such processes of controlling the harmful formaldehyde volatile, photocatalytic oxidation has been considered a green and economical technology owing to its simple process, low energy consumption, and thorough degradation of pollutant [13]. For the numerous catalytic materials, anatase titanium dioxide (TiO₂) was regarded as the most effective light-induced catalytic material owing to its high cost-performance ratio, excellent chemical stability, and good ultraviolet (UV) resistance. However, traditional anatase TiO₂ catalysts generally need to initiate under high-energy UV lamps or limited UV light in the sunlight. The visible light in daylight cannot play an effective catalytic activity [14]. Additionally, pristine anatase TiO₂ cannot degrade indoor formaldehyde in the darkness, which limits its practical application. Considering the rich indoor visible light in the daytime and long hours for people sleeping at night, it is necessary to modify the anatase TiO₂ to widen its photo-responsive wavelength, thereby resulting in a good catalyst with a visible light and darkness response for degrading formaldehyde.

The photocatalytic decomposition of formaldehyde volatiles has been difficult because of the common deactivation of modified anatase TiO₂ composite, especially in visible and dark environments. Luminescent ions and nanomaterial doping processes were vital methods for the modification of long-lasting phosphors [15]. Various strategies (metal deposition, graphite carbon nitride modification, and phosphor decoration) have been developed for the visible-light modification of TiO₂-based photocatalysts [16–18]. However, the most traditional graphite carbon nitride and metal dots are expensive or contain toxic metal-ions, which are harmful to human health in indoor applications. Carbon dots (CDs), as a classic fluorescent nanomaterial, have gained increasing attention for bio-imaging, sensing, and catalytic fields because of their low toxicity, wide absorption spectrum, good electronic conductivity, and doped-dependent photoluminescence (PL) behaviors [19–21]. Till now, hydrothermal synthesis of CDs from biomass (wood, grass, and bamboo particles) has been proven to be a low-cost and effective strategy, thereby producing doped CDs with diverse absorption in visible light regions [22]. The fluorescent CDs within 10 nm in size generally have small band gaps (≤ 2.0 eV) owing to their nanoscale sizes and quantum effects, which presents great potential in catalysis fields [23]. For the CDs/TiO₂ composite photocatalyst, the introduction of CDs is conducive and enhances the photo-induced electron transfer of the TiO₂ system. Gao et al. [24] synthesized a catalyst with lignin-based CDs and TiO₂ sheets, which enhanced both the adsorption capacity and activity of the carbon dioxide. Martins et al. [25] applied nitrogen (N) doped CDs to prepare composite catalysts, which exhibited good degrading activity of NO_x under visible light irradiation. However, not all CDs can contribute to visible-light catalytic activity. CDs with N- and phosphorus (P)-doping can help the adsorption of molecular oxygen and offer the high efficiency of CDs/TiO₂ composites for decreasing organic pollution [26].

Moreover, it is crucial to prolong the lifetime of the composite catalyst system and further enhance its comprehensive activity in photocatalysis. SrAl₂O₄: Eu²⁺, Dy³⁺ (SAO) is a typical rare-earth strontium aluminate long-afterglow self-luminous phosphor, which is beneficial for energy harvesting in the daylight (UV or visible light) and emitting long-lasting visible light under dark conditions. It is widely applied in our lives, such as in indication marking, luminescence sensing, luminous plastic, the ceramic industry, and photocatalytic fields [27–30]. The composites with SAO phosphors generally store light energy during the daytime and emit visible light for minutes to hours in the dark environment. However, SAO phosphors tend to cause hydrolysis under humid or watery environments, which accelerates the crystalline destruction of SAO particles and reduces their self-luminous activity. Moreover, the band gaps of SAO phosphors are obviously higher than those of typical CDs and TiO₂ photocatalysts [31]. In our previous report, we showed that a sol-gel-induced SiO₂-coating layer on SAO phosphors can prevent the degradation of O-Sr-O bonds even in an aqueous condition [32]. Therefore, a buffer binding

layer modification is necessary to improve the water resistance and adhesion with other catalytic nanoparticles.

To our knowledge, there are no reports in the literature concerning the use of CDs/TiO₂/SAO composites in the photocatalytic removal of formaldehyde and other indoor organic volatiles. Moreover, studies of the oxidation of formaldehyde using a photocatalyst with long-lasing visible light activity are still scarce. The objective of this research was to develop a novel self-luminous wood coating with carbon dots (CDs)/titanium dioxide (TiO₂) nanomaterial coated SrAl₂O₄: Eu²⁺, Dy³⁺ (CDs/TiO₂@SAO) composite for the long-term degradation of formaldehyde. In this work, a novel strategy for the reasonable utilization of CDs from wood sanding dust and the doped composite catalyst on wood surfaces for the degradation of formaldehyde was explored. Fluorescent CDs were first prepared by the hydrothermal process of wood sanding dust and then sol-coated with TiO₂ and SAO phosphor to obtain a core-shell CDs/TiO₂@SAO composite coating on the wood. The photo-oxidation effect of formaldehyde under UV irradiation, visible light, and a dark environment was demonstrated. The potential mechanism for the enhanced photocatalytic activity of CDs/TiO₂@SAO composite coating has been further discussed.

2. Materials and Methods

2.1. Materials

Anatase TiO₂ powder with a 25 nm primary particle size, tetraethyl orthosilicate (TEOS, 98%), citric acid monohydrate (CA), ethanol (C₂H₅OH), and pH buffer solutions with a pH of 3.0 were purchased from Aladdin. SAO phosphors with an average particle size of 6.2 μm were obtained by Lu Ming Luminescent Materials Co., Ltd. (Liaoning Province, China). Wood sanding dust waste (moisture content was about 4.6%) and the UV-initiated aqueous curing paint were supplied by Ruixin Decoration Co., Ltd. (Zhejiang Province, China). Tris (hydroxymethyl) phosphine oxide (THPO, 85%) was purchased from Shanghai Gaoming Co., Ltd. (China). The fir wood (*Cunninghamia lanceolata* (Lamb.) Hook.) samples were supplied by the Chinese Academy of Forestry (Beijing, China). Deionized water was used to extract the wood sanding dust and prepare solutions for all the experiments.

2.2. Synthesis of N,P-Doped CDs from Recycling Wood Sanding Dust

The N,P-doped CDs were synthesized from recycled sanding dust via a two-step hydrothermal process. Shortly, sanding dust and 150 g of deionized water were mixed with a solid-to-liquid ratio of 1/12.5. The mixture was then transferred to autoclaves (250 mL) in an oven (165 °C) and pre-extracted for 1.0 h. The brownish pre-extraction (160 g) was filtered with a Syringe Filter (0.45 μm) and then transferred to a 250 mL sealed reactor with 8 g of THPO. The reactor was then processed at 220 °C for 6 h for carbonization. The resulting solution was cooled down, centrifuged at 8000 rpm for 8 min, and vacuum freeze dried to obtain N,P-doped CDs. For comparison, the CD materials without P-doping were also synthesized using the sanding dust directly in the same process, denoted as NCDs.

2.3. Formation of CDs/TiO₂@SAO Composite Photocatalyst

The modified CDs/TiO₂@SAO composite photocatalyst was obtained via a silica sol-gel method. Specifically, TEOS (0.8 mL) was mixed with ethanol (9 mL) and pH 3.0 buffer (2 mL) in a 65 °C water bath for 2 h. Uniform pre-dispersion of CDs/TiO₂ was prepared by adding 0.05 g of TiO₂ and 0.1 mg of N,P-doped CDs into ethanol (20 mL) and buffer (3 mL) solutions. Furthermore, CDs/TiO₂ dispersions were transferred to the TEOS sol and vigorously stirred for 45 min at 65 °C. Subsequently, SAO phosphors (0.8 g) were added and continually stirred for 15 min, in order to obtain uniform gel-coated phosphors. Finally, the obtained particles were washed using an alcohol solution until the upper centrifugal liquid was colorless under a 365 nm UV-lamp. The cleaned precipitation was then dried at 50 °C for 24 h to obtain the CDs/TiO₂ modified SAO core-shell phosphors, denoted as CDs/TiO₂@SAO.

2.4. Formation of Photocatalytic Wood Coatings with CDs/TiO₂@SAO Composite

The pre-weighed phosphors (3.6 g) were added to a water-based photo-curing paint (50 g) with mechanical stirring for 15 min to obtain a uniform suspension. The self-luminous suspension was then sprayed on a piece of wood (100 × 45 × 5 mm³) using a spray gun with a nozzle diameter of 0.5 mm under an air pressure of ~0.7 MPa. Subsequently, the samples after spraying treatment were processed using a UV-curing device to obtain photocatalytic wood materials. The coating thickness was controlled within 80–100 μm to maintain the apparent color of wood. For comparison, other modified wood materials with the pristine TiO₂ and SAO coatings were prepared using similar processes. Finally, all the wood samples in the absence and presence of catalytic coating were placed in a room (20 °C; 55% relative humidity) for further tests. Figure 1 shows the preparation process of the CDs/TiO₂@SAO core-shell composite and the resulting wood materials with long-term photocatalytic coatings.

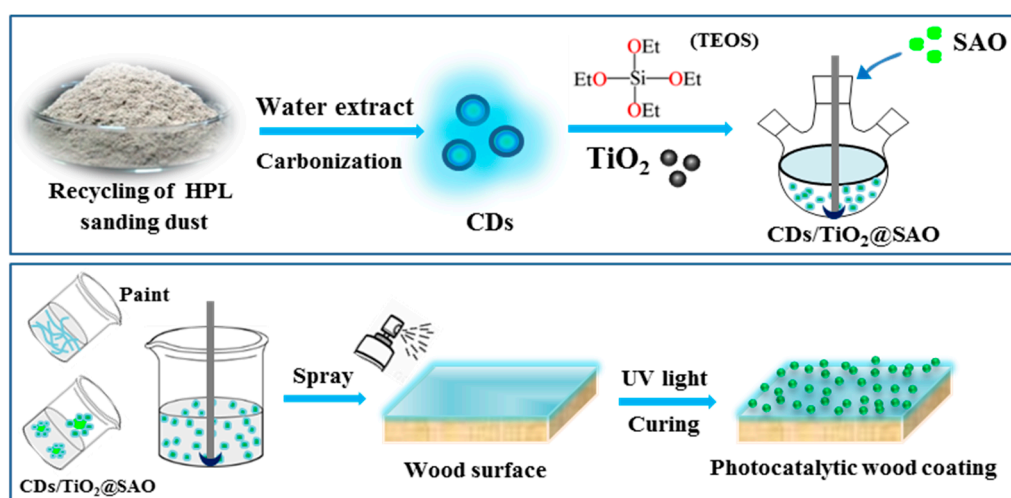


Figure 1. Preparation of the CDs/TiO₂@SAO core-shell microspheres and the long-lasting photocatalytic wood coatings.

2.5. Material Characterization

Morphologies of the dispersed CDs and modified SAO phosphors were observed using a FEI Tecnai G2-F30 transmission electron microscope (TEM; Hillsboro, USA). A drop of highly diluted CDs aqueous solution or phosphor dispersion was placed onto the copper grid with a holey amorphous carbon film and left to dry in the air until being used for the TEM microscope. High-resolution TEM (HRTEM) images were used to analyze the lattice fringes of CDs. The surface topographies of CDs in three-dimensional (3D) and two-dimensional (2D) modes were performed using a Bruker atomic force microscope (AFM; Karlsruhe, Germany). Fourier-transform infrared (FTIR) spectra of the solid samples were recorded using a Nicolet IS10 spectrometer (Massachusetts, USA). Thermogravimetric analysis (TGA) curves of the samples were obtained using a Netzsch TG STA 449 F5/F3 analyzer (Bavaria, Germany) in nitrogen atmosphere using a heating rate of 10 °C/min up to 800 °C. A Hitachi 8020 scanning electron microscope (SEM; Tokyo, Japan) equipped with an energy-dispersive spectroscopy (EDS) detector was used to observe the morphologies of the phosphors and wood coatings and to evaluate the distribution of catalyst using the element-mapping mode with the same scanning time. Powder X-ray diffraction (XRD) patterns were recorded using a D8 XRD meter (Bruker, Germany) with a scan rate of 8°/min. PL spectra of the CDs and phosphor samples were recorded using an FLS100/FS5 spectrometer (Edinburgh, UK). The same quality of phosphors in the presence and absence of CDs/TiO₂ coatings was used for the comparative analysis of the PL emission. The Commission Internationale de L'Éclairage (CIE) coordinates of luminescent samples are calculated using the PL spectra. The PL decay status and afterglow lifetime were monitored

in the spectrometer (excitation illumination: 1000 lx, excitation time: 15 min). The emission spectra of the indoor compact fluorescent light (CFL) and the sunlight (116°20' E, 39°56' N) at daytime were obtained using an S-5000 spectrometer (Hamamatsu, Japan). The absorbance spectra of CDs solutions were measured using a GD-54T UV-visible (UV-vis) spectrometer (Shanghai, China). The UV-vis diffuse reflectance spectra of photocatalyst were performed using a Shimadzu UV-3600 spectrometer (Tokyo, Japan).

2.6. Photocatalytic Activities Characterization

Volatile formaldehyde represents a major organic pollutant of VOCs in indoor environments, and here it was chosen as a representative to evaluate the photocatalytic behaviors. All the photocatalytic experiments were carried out in a closed reactor with a volume of ~100 L to simulate the dynamic degradation behaviors of volatile formaldehyde pollutants. Three different light source conditions, such as a 365 nm UV lamp, visible light from a compact fluorescent light (CFL, 8 W), and a dark environment, were chosen to analyze the catalytic efficiency of functional wood materials. The schematic of the reactor for formaldehyde degradation in the presence and absence of a light source is shown in Figure 2. Prior to the experiment, the reactor was placed in a room (20 °C; 55% relative humidity) under the darkness for more than 24 h. Subsequently, the wood materials were put on a suspended wire mesh with a total area of ~135 cm², and the required quantity of formaldehyde was injected into the closed reactor. Typically, the initial concentration of volatile formaldehyde in the reactor was kept at ~0.2 mg/m³ for all the experiments. When the formaldehyde concentration reached a dark-adsorption equilibrium, photocatalysis experiment was started by turning on the UV lamp or visible light.

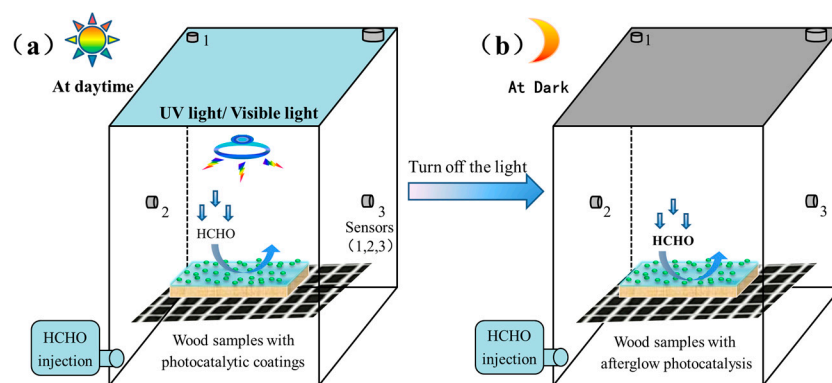


Figure 2. Schematic of the photocatalytic reactor for formaldehyde degradation: (a) photocatalysis under light source conditions (UV light or CFL visible light); (b) photocatalysis in the darkness.

Specifically, for the long afterglow photocatalytic experiment in the darkness, the wood samples with CDs/TiO₂@SAO composite coating were pre-exposed to CFL visible light for 45-min before the formaldehyde injection. The degradation efficiency of formaldehyde was calculated by $(C_0 - C_t)/C_0$, where C_0 is the reactant concentration after adsorption equilibrium and C_t is the reactant concentration after irradiation from light or preservation in darkness for a certain time. For comparison, the wood materials with pristine TiO₂ and SAO composite coatings were also treated in the same process for evaluation of the degradation efficiency owing to the CDs and SAO modifications.

3. Results and Discussions

3.1. Characterization of Fluorescent N,P-Doped CDs

The TEM and HRTEM characterization results of N,P-doped CDs (Figure 3a,b) show that the as-prepared CDs are uniform in size and well dispersed. The particle size distributions of N,P-doped CDs were mainly in the range of 2–7 nm with an average size of 4.5 nm (100 random nanoparticles were accounted for CDs) (Figure 3c). HRTEM images of the N,P-doped CDs (Figure 3b) reveal that most of the CDs are crystalline with well-resolved

lattice fringes. The inset lattice spacing in the HRTEM image was ~ 0.21 nm, indicating that the spacing array can be assigned to the crystalline phase (1120) of graphite, which is consistent with our previous report on biomass-derived CDs [20]. The AFM images (Figure 3d,e) also indicate the formation of well-dispersed particles in spherical shape. Moreover, the hyperfine nanoparticle deposition depth of CDs dispersion was mainly located in the range of 6.5–8.2 nm (Figure 3f), which indicates the nanoscale roughness was deposited owing to 1–4 layers of well-dispersed CDs.

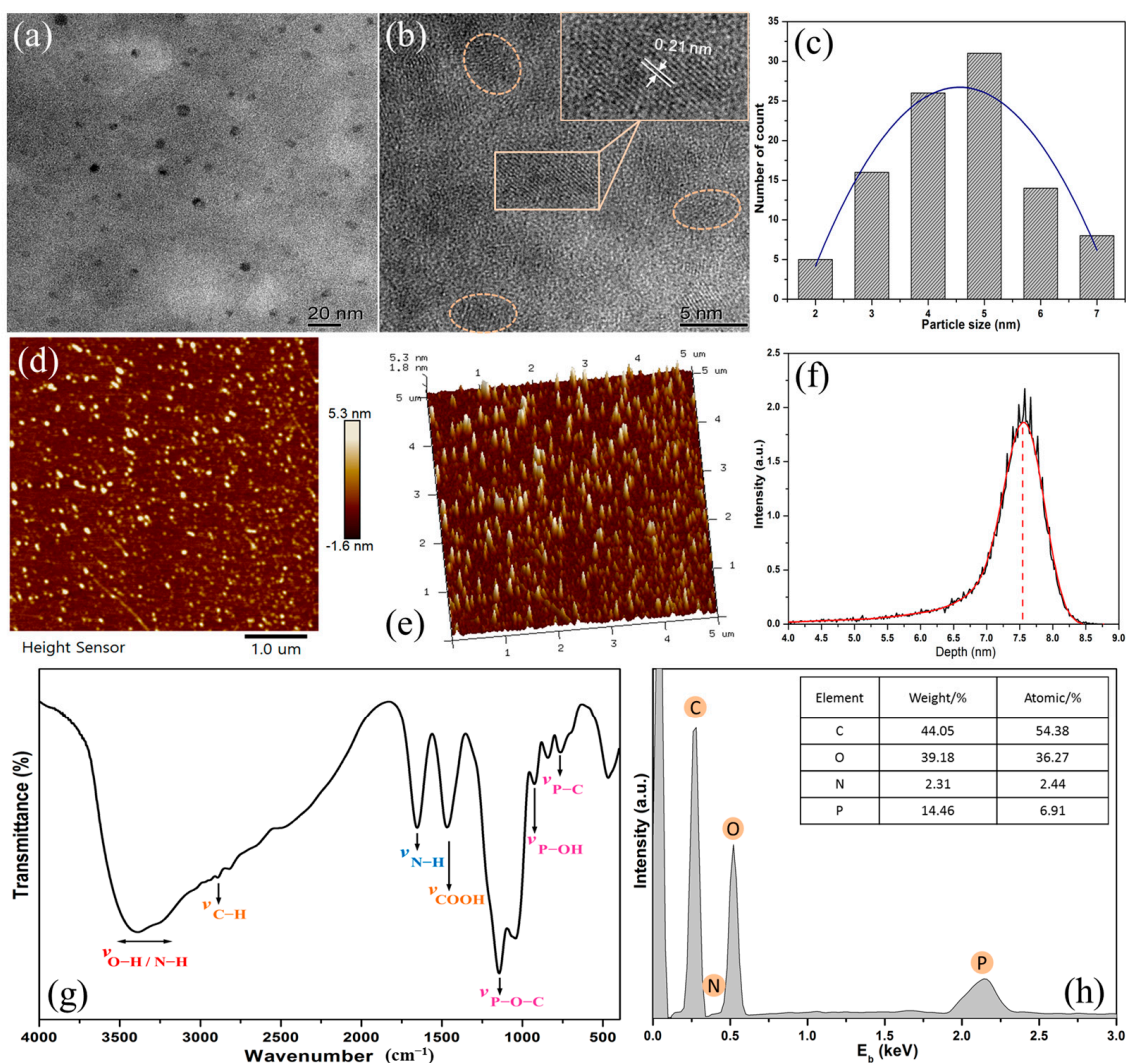


Figure 3. (a) TEM and (b) HRTEM images of N,P-doped CDs. Inset is the lattice fringes, the color circles are the magnification of CDs; (c) Histogram image of N,P-doped CDs (the color curve is the average particle size distribution); (d) 2D-AFM map, (e) 3D-AFM image, and (f) nanoparticle deposition depth of the N,P-doped CDs dispersion; (g) FTIR spectrum and (h) EDS diagram of the N,P-doped CDs.

The chemical groups of the N,P-doped CDs were further analyzed using FTIR (Figure 3g). The FTIR spectra reveal that the N,P-doped CDs were highly functionalized with oxygen-containing groups. The broad peak around $3490\text{--}3050\text{ cm}^{-1}$ is ascribed to the stretching vibrations of the O–H or N–H bonds, indicating the abundant existence of hydroxyl and carboxyl groups in the CDs [33]. The shoulder peak at 2910 cm^{-1} is attributed to various C–H vibrations. The three sharp peaks at 1622 , 1495 , and 1176 cm^{-1} are attributed to the vibration modes of N–H, COOH, and P–O–C, respectively [34]. Other peaks corresponding to P–OH (885 cm^{-1}) and P–C (762 cm^{-1}) have also been observed. These

results imply that abundant amino, carboxyl, and phosphate groups were present on the surface of N,P-doped CDs. The EDS diagram and elemental contents of N,P-doped CDs further indicate that the CDs contain C, O, N, and P elements at concentrations of 44.05, 39.18, 2.31, and 14.46 wt%, respectively (Figure 3h). Thus, these results indicate that the N,P-doped CDs are mainly composed of carbon-core and active surface groups owing to their intrinsic C, O, N, and P elements.

3.2. Characterization of CDs/TiO₂@SAO Core-Shell Composite Photocatalyst

A novel coated phosphor of long-lasting afterglow SAO decorated with CDs/TiO₂ nanoparticles was prepared using a simple sol-gel coating method. Figure 4a shows the typical crystalline structure of dispersed TiO₂ in a rectangular shape. Prior to the coated modification of SAO, the microstructure of CDs/TiO₂ composites was evaluated (Figure 4b). It is clear that apparent agglomerations occurred between TiO₂ and CDs nanoparticles due to the abundant hydroxyl functional groups on the CDs and TiO₂ nanoparticles, which is beneficial to the further modification of CDs/TiO₂ composites on the surface of SAO phosphor via a sol-gel process. Figure 4c shows the TEM image of CDs/TiO₂@SAO phosphor. It clearly illustrates the successful coupling of nano-scaled coating onto the SAO particles.

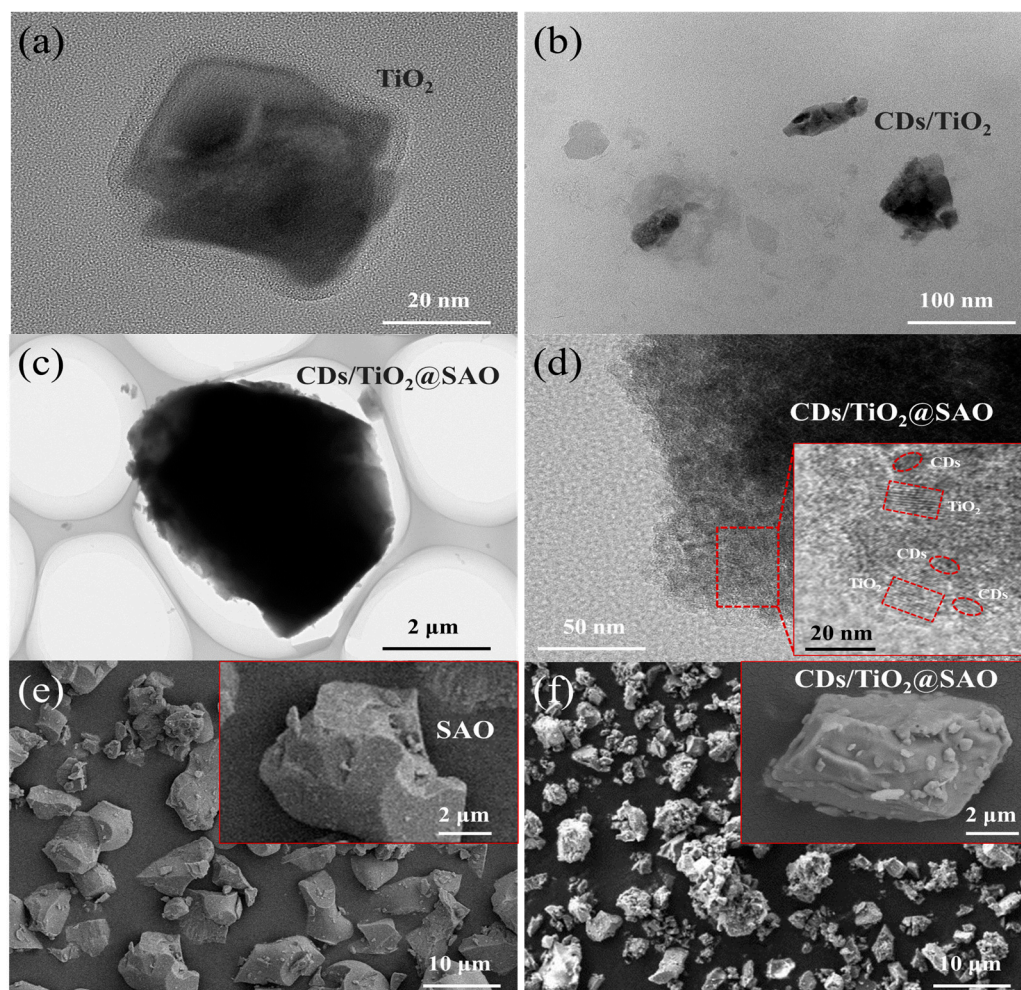


Figure 4. TEM images of (a) TiO₂, (b) CDs/TiO₂, and (c) CDs/TiO₂@SAO composite photocatalyst. (d) HRTEM of CDs/TiO₂@SAO. Inset is the lattice fringes of CDs/TiO₂ coating on the SAO particle; SEM images of (e) uncoated SAO and (f) CDs/TiO₂ modified SAO phosphors. Inset is the magnified image.

The HRTEM of CDs/TiO₂ composites further reveals that smaller spherical particles of CDs intermixed with larger rectangular crystals of TiO₂ were clearly identified due to the different lattice fringes, as shown in Figure 4d. The clear lattice fringe of 0.35 nm was assigned to the (101) diffraction plane of the anatase phase of TiO₂ particles, while the fringe of 0.21 nm matched that of CDs [35]. These results fully proved that both CDs and TiO₂ nanoparticles were successfully coated on the surface of SAO phosphor after the sol-gel strategy. The SEM images of uncoated SAO and CDs/TiO₂-coated SAO phosphors are shown in Figure 4e,f. It was apparent that the surface of coated SAO particles became rougher than that of uncoated SAO, which further illustrates that a protective coating layer was formed on the SAO particles. All these results further confirm that the fluorescent CDs and photocatalytic TiO₂ nanoparticles were uniformly coated on the afterglow SAO phosphors.

The structure and thermal decomposition of the SAO phosphors in the absence and presence of CDs/TiO₂ coating layer were further identified by the XRD and TGA analyses. Figure 5a exhibits the XRD patterns for pristine TiO₂ and the CDs/TiO₂ nanoparticles coated on the SAO phosphors. Both the anatase TiO₂ and SAO particles were crystalline with typical characteristic peaks. Compared with TiO₂, the XRD pattern of CDs/TiO₂ after CDs modification exhibits similar peaks, whereas the intensity for CDs/TiO₂ shows a slight increase at 20–30° compared with the baseline. This observation is consistent with our previous result that hydrothermal biomass-based CDs were primarily amorphous structures with wide diffraction [20]. For the coated CDs/TiO₂@SAO photocatalyst, the characteristic peaks at (011), (211), and (031) for SAO weakened with additional CDs and TiO₂ coatings were presented [32]. A new little peak assigned to the (101) crystal of TiO₂ at 25.4° also appeared, whereas other characteristic peaks of TiO₂ were not obvious owing to their overlapping with the strong peaks of SAO phosphors. This confirms that the CDs/TiO₂ coating on SAO particles has no adverse effect on the typical crystalline structure of TiO₂ and SAO phosphors.

The TGA and DTG results of modified phosphors are shown in Figure 5b,c. The TGA curves of unmodified SAO and TiO₂ showed a rapid mass loss at 40–150 °C and then remained constant up to 800 °C. It is mainly attributed to the occurrence of adsorbed water owing to the hydroxyl groups on the microspheres and nanoparticles. For the CDs/TiO₂@SAO composite photocatalyst, the decomposition process presents three stages. The steep decomposition peak centered at 150–255 °C was ascribed to the elimination of surface groups on CDs; this is consistent with the pyrolysis result of biomass-based CDs [20]. As the temperature continues to rise from 250 °C to 550 °C, the continuous mass loss (~8.6%) is consistent with the fluctuating pyrolysis of silane-containing polymers physically bonded to the surface of SAO particles [28]. The inset in Figure 5c is the photographs of CDs/TiO₂@SAO at daylight and dark conditions after pyrolysis. The strong green emission of photocatalyst at night illustrates that the self-luminous activity of CDs/TiO₂@SAO can be maintained even after 800 °C thermal treatment.

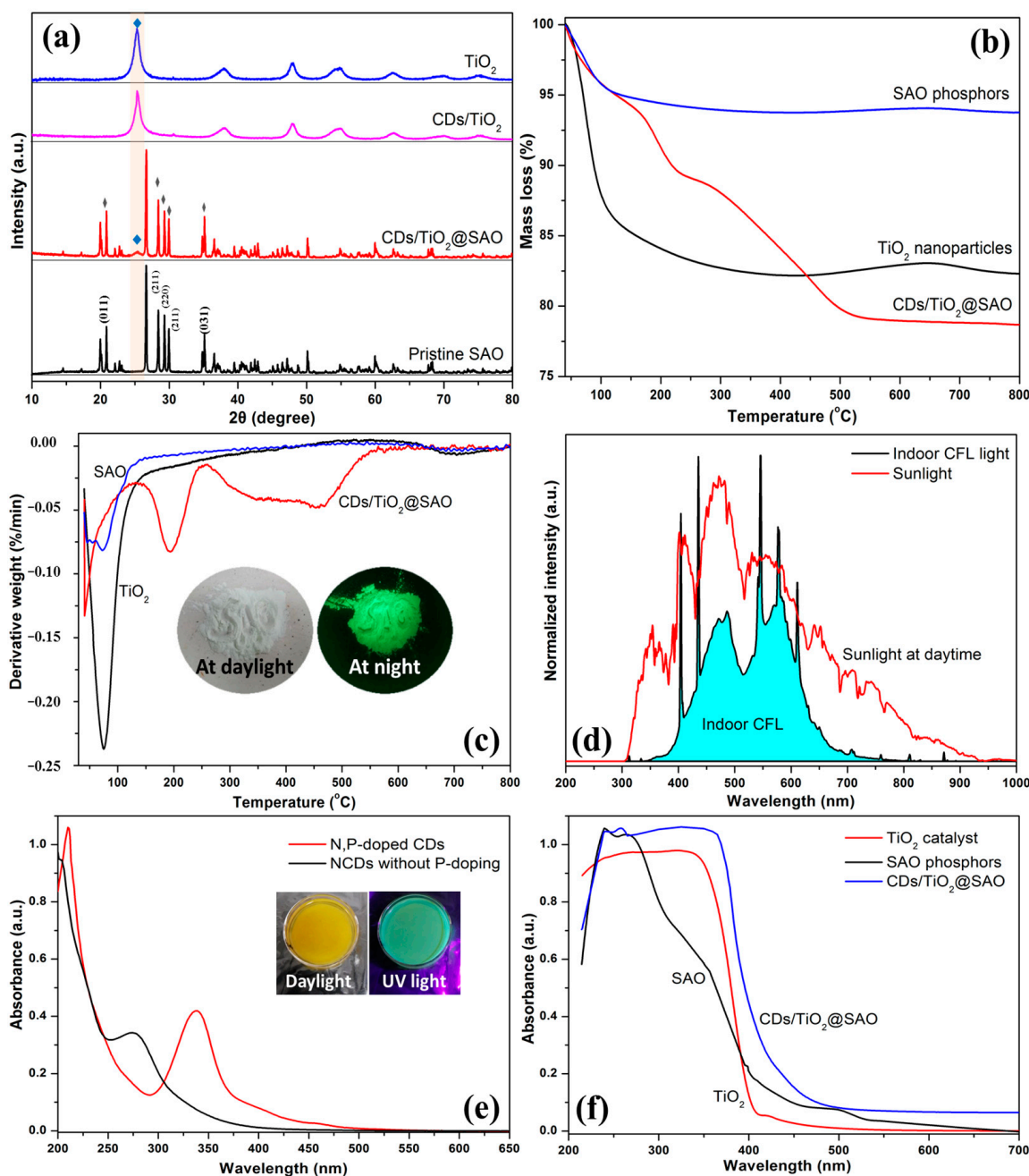


Figure 5. (a) XRD patterns of TiO₂ and SAO phosphors with CDs coated modification; (b) TGA and (c) DTG of SAO, TiO₂, and coated CDs/TO₂@SAO particles. Inset is the photographs of CDs/TO₂@SAO at daylight and dark condition after pyrolysis; (d) Emission spectra for the indoor CFL light and the sunlight at daytime; (e) UV-vis absorption spectra of different CDs. Inset was N,P-doped CDs solution under the daylight and 380 nm UV-lamp; (f) UV-vis diffuse reflectance spectra for different phosphors.

The typical emission spectra of the indoor CFL light and the sunlight at daytime are shown in Figure 5d. It is clear that sunlight is composed of strong UV light (315–400 nm), visible light (400–770 nm), and weak near-infrared light (770–900 nm). Compared the sunlight, the spectrum of indoor CFL is in the range of visible light at 400–700 nm, including blue light (400–485 nm), blue-green light (485–510 nm), green light (510–565 nm), and other wavelengths of light. Therefore, the key to improving the photocatalytic activity of wood coatings is to broaden the response of the photocatalyst in an indoor visible light environment. The optical properties of the samples were analyzed with the UV-vis spectra.

The UV-vis absorption spectra of CDs in the presence and absence of P-doping are shown in Figure 5e. The maximum absorption peak of the N,P-doped CDs was observed at 340 nm, which is attributed to the $n - \pi^*$ transitions of surface C=O and C–N bonds [36]. Whereas the shoulder at 265 nm is represented by the $\pi - \pi^*$ transition of the aromatic C=C bond from the carbon core. Compared with the NCDs without P-doping, the UV-vis spectrum of N,P-doped CDs also exhibits broad tailing at 370–475 nm, which helps absorb additional visible light owing to the oxygen-related P-doping groups and surface defects in the N,P-doped CDs [37]. Figure 5f shows the UV-vis diffuse reflectance of pristine TiO₂, SAO phosphor, and CDs/TiO₂@SAO composite photocatalyst. It can be seen clearly that the CDs/TiO₂@SAO composite has a wider absorption band in the wavelength range of 400–700 nm, whereas the pristine TiO₂ only exhibits a strong UV optical absorption edge at 400 nm corresponding to the wide band gap (~3.2 eV) as referenced by other researchers [38]. It is mainly due to the strong absorption of N,P-doped CDs and SAO phosphor in the UV-vis region, which may change the charge transfer process between the CDs and TiO₂ in the coupling compound materials. Therefore, the optical absorption of the TiO₂ system was extended to the UV-vis region by incorporation of the N,P-doped CDs and the self-luminous SAO phosphor, thus enhancing the photocatalytic degradation efficiency of the CDs/TiO₂@SAO hybrid system for formaldehyde pollutant.

The PL emission spectra of N,P-doped CDs aqueous dispersion at different excitation wavelengths (340–490 nm) are displayed in Figure 6a. The PL intensity distinctly increased as the excitation wavelength increased from 340 nm to 430 nm and subsequently decreased with the increasing excitation wavelengths up to 490 nm. The maximum PL emission of the N,P-doped CDs appeared at λ_{ex} of 430 nm (blue), which is different from our previous biomass CDs without P-doping [20]. It was expected to expand the visible light absorption of CDs and enhance the photocatalytic activity of the CDs composite under visible lights. Moreover, the CIE chromaticity diagram of the N,P-doped CDs solution is present in Figure 6b. Especially, the PL emission of the SAO phosphor presented absolute green light with the CIE coordinates of 0.226 (x) and 0.469 (y), whereas the N,P-doped CDs depicted multicolor behavior tuned from 455 nm (blue) to 570 nm (yellowish-green). The tunable emission result of CDs is mainly attributed to the quantum effects and electron transitions between the σ and π molecular orbitals owing to the N,P-doping modification, which is consistent with our previous N-doping biomass-based CDs [20].

The excitation spectra of SAO phosphor (detected at 510 nm) and PL emission spectra (excited at 350 nm) under a dark environment of modified SAO phosphors are shown in Figure 6c. The excitation spectrum of SAO phosphor presented a continuous wide band centered at 360–428 nm, indicating that the SAO phosphors were effectively excited by UV light to visible light. It is attributed to the typical $4f^65d^1$ to $4f^7$ -transition of Eu²⁺ ions in SAO crystals [39]. Furthermore, the PL emission intensity of CDs/TiO₂@SAO modified photocatalyst was ~5% lower than that of the SAO sample, while the peak for the SAO phosphors before and after modification was unchanged. It can be attributed to the slight light scattering activity due to the CDs and TiO₂ nanoparticles on the core-shell SAO surface owing to the sol-gel modification. The long afterglow luminescence decay curves of CDs/TiO₂@SAO and SAO phosphors are shown in Figure 6d. After removal of excitation irradiation, the two phosphors presented a strong initial brightness up to 1635 and 1855 mcd/m² in the dark environment. Subsequently, a rapid decay was occurred during the first 2 min and then a slow decay behavior up to 3600 s. The brightness of the CDs/TiO₂@SAO and SAO phosphors at 3600 s (6 h) was still 3.19 mcd/m² and 3.55 mcd/m², respectively. These values were obviously higher than the recognition minimum limit of 0.32 mcd/m² by the naked eye at night. The afterglow luminescence of CDs/TiO₂@SAO was not obviously changed after the CDs and TiO₂ coating, indicating that the sol-gel CDs/TiO₂ coating layer was suitable for the modification of SAO phosphors. Therefore, these core-shell microspheres with self-luminous SAO phosphors and CDs/TiO₂ photocatalysts have a vast potential application in photocatalytic degradation under indoor visible light and dark environment.

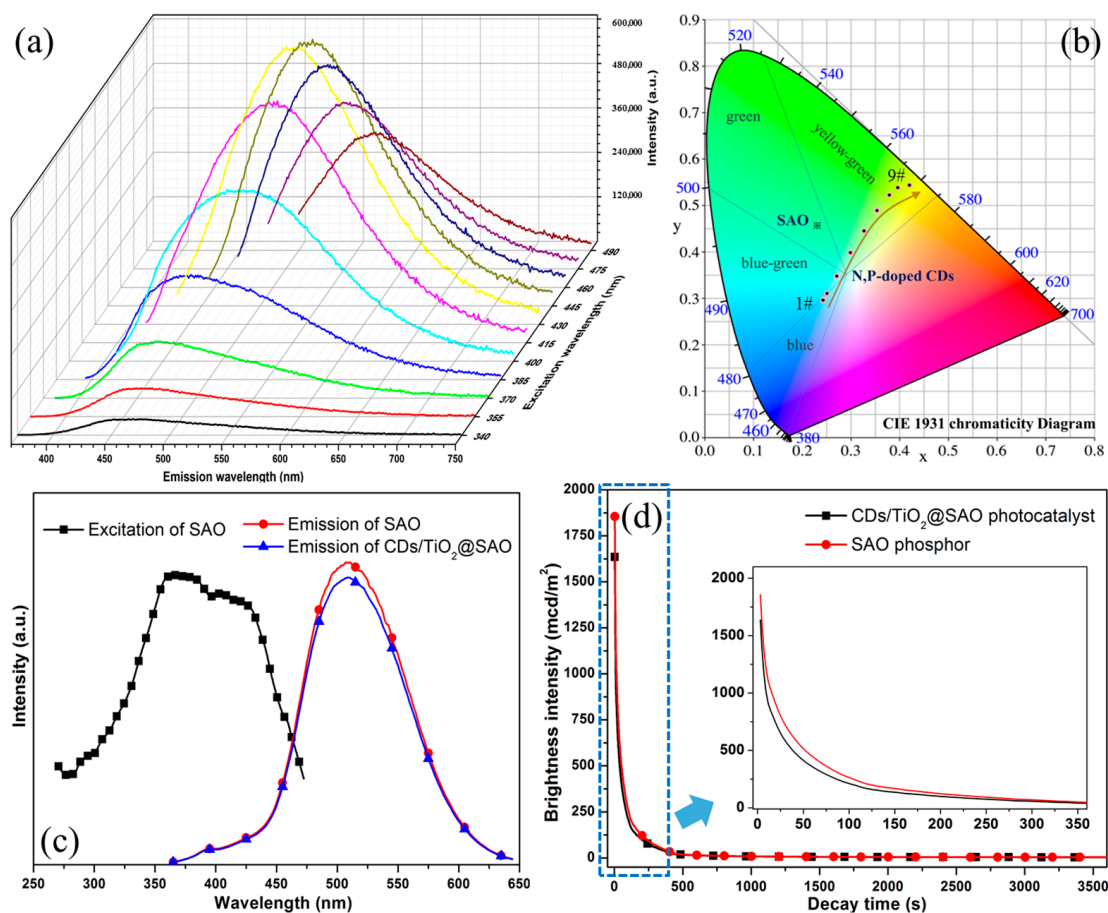


Figure 6. (a) PL emission spectra of N,P-doped CDs with λ_{ex} ranging in 340–490 nm (excitation gradient of 15 nm). The color curves are the emission spectra with different excitations; (b) CIE chromaticity diagram of SAO and N,P-doped CDs solution, where samples 1# through 9# correspond to PL emission with λ_{ex} ranging in 340–490 nm (excitation gradient of 15 nm); (c) Excitation spectrum of SAO and the PL emission of CDs/TiO₂@SAO; (d) Long-afterglow decay lifetime of the CDs/TiO₂@SAO under dark environment (detected after 365 nm irradiation).

3.3. Morphologies of Wood Coatings with CDs/TiO₂@SAO Composite Photocatalyst

The composite photocatalyst was further introduced to the typical UV-curing paint matrix to prepare wood coatings. Figure 7 shows the surface microstructure of the control wood and functional wood materials after the UV-curing paint coating and CDs/TiO₂@SAO coating. For the control wood sample without surface coating modification (Figure 7a,d), it was clear that the wood shows a porous surface with a large number of tracheid lumens, wood rays, and cracks in micrometer scale, which is beneficial for the filling and adhesion of the paint substrate with the CDs/TiO₂@SAO particles. The paint coatings were observed clearly on the wood samples (Figure 7b,e), and covered the original surface morphology of the porous wood skeleton to form a relatively smooth film. This can be explained by the fact that the paint polymers adhere to the wood surface owing to their strong binding effect. Additionally, the composite paint coatings with CDs/TiO₂@SAO photocatalytic particles were attached tightly to the wood (Figure 7c), suggesting a good filling and adhesion of the coatings to the porous wood skeleton. The SEM image of the CDs/TiO₂@SAO composite photocatalytic coatings in higher magnification indicated that random particles were anchored tightly by the film-forming paint (Figure 7f). To further determine the distribution of the CDs/TiO₂@SAO photocatalyst on the coatings, the EDS elements mapping of the typical elements for SAO, TiO₂, and CDs were examined (Figure 7g–j). The EDS elements mapping clearly showed the existence of Sr, Si, C, and N in the photocatalytic coatings, and all these elements were distributed uniformly in the composite coatings. These EDS results

were in line with the results obtained from the SEM of coatings. The uniform photocatalytic coatings on wood substrate is essential for the practical indoor application in capturing and eliminating the volatile formaldehyde pollution.

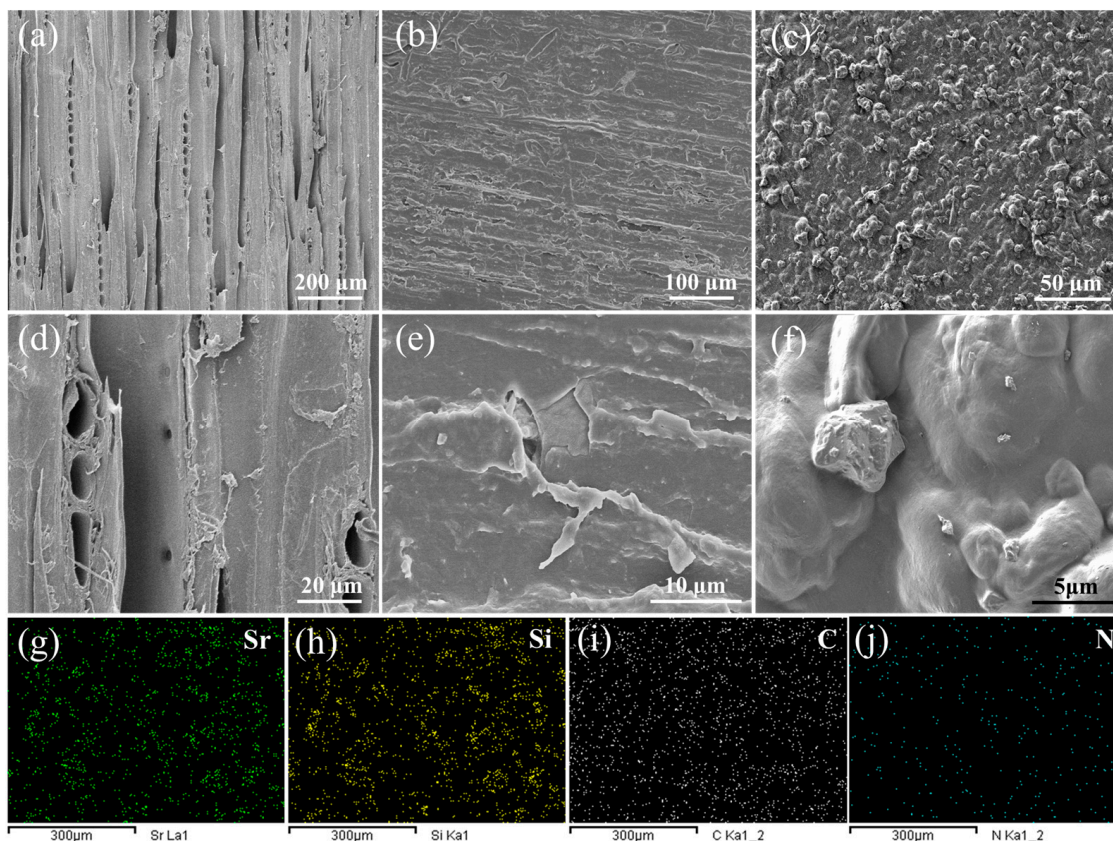


Figure 7. Morphologies and EDS scans of the coated wood surfaces: (a,d) Control wood; (b,e) Wood with pristine paint coatings; (c,f) Photocatalytic wood with CDs/TiO₂@SAO composite coatings; (g–j) Element-mapping distributions of Sr, Si, C, and N, respectively.

3.4. Photocatalytic Activity and Mechanism of Formaldehyde Reduction

Volatile formaldehyde represents a major organic pollutant in indoor environments, and here it was chosen as a representative to verify the degradation behaviors of the functional wood materials with CDs/TiO₂@SAO composite coatings. Firstly, the wood samples were put into the reactor in darkness for 24 h to eliminate the long-lasing afterglow fluorescence effect. Prior to irradiation, quantitative formaldehyde pollution was injected into the reactor ~30-min in advance to ensure the adsorption-desorption equilibrium. Figure 8a presents the formaldehyde degradation curves of the wood materials with CDs/TiO₂@SAO composite coatings under continuous exposure to visible light ($\lambda \geq 400$ nm). As shown in Figure 8a, the blank experiment presents that the self-degradation activity of the wood with pristine SAO and TiO₂ coatings can be ignored owing to a slight decrease even after 160-min irradiation with visible light, which is mainly contributed to the slight adsorption effect owing to the porous structure of wood materials. The wood with CDs/TiO₂ and CDs/TiO₂@SAO composite coatings shows higher photocatalytic activities than that of the pristine TiO₂ and SAO coatings under the visible light condition. It is probably due to the enhancement of electro-hole separation efficiencies in the CDs/TiO₂ and CDs/TiO₂@SAO composites [40,41]. For the CDs/TiO₂@SAO composite coatings, the degradation reaction of formaldehyde reached ~60% in a 160-min cycle, which implies that the CDs/TiO₂@SAO composite is a promising candidate for indoor volatile pollutants.

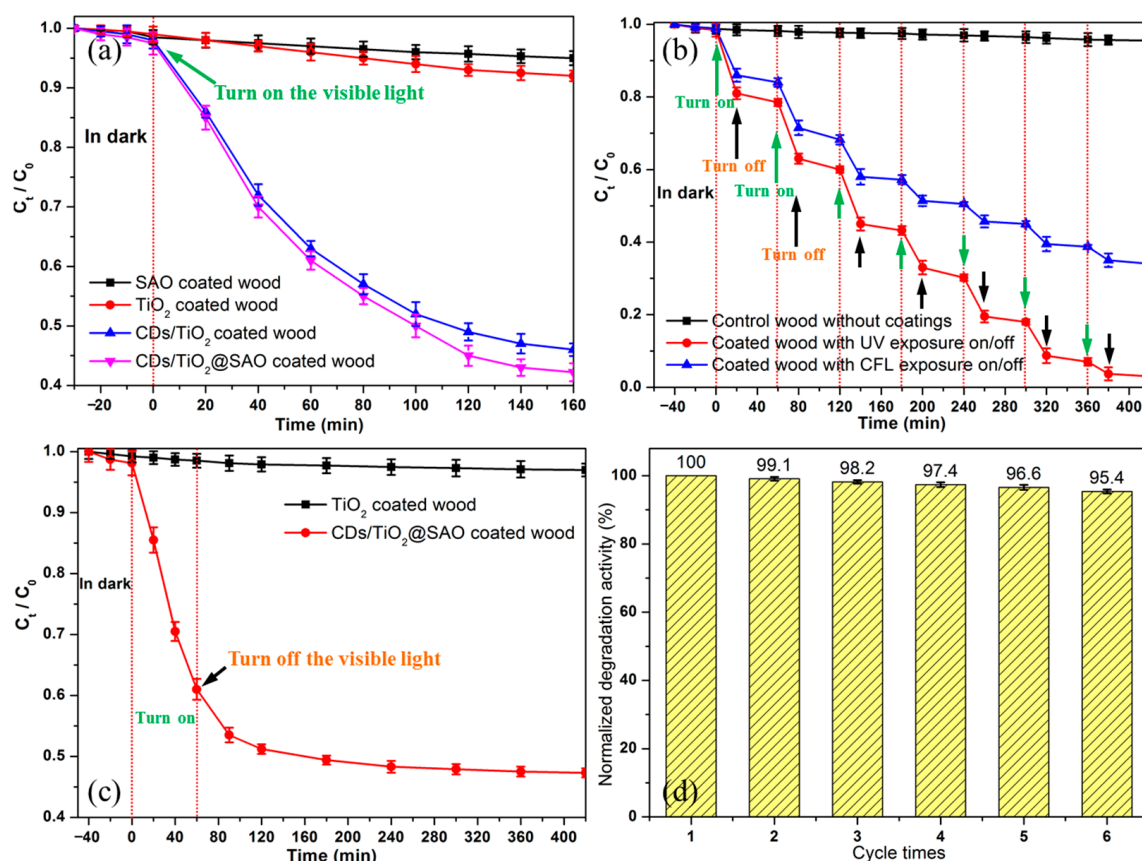


Figure 8. Photocatalytic activities of the CDs/TiO₂@SAO composite coated wood materials for the degradation of formaldehyde with different irradiations: (a) Continuous CFL visible light ($\lambda \geq 400$ nm) exposure; (b) Intermittent UV ($\lambda = 365$ nm) or CFL visible light exposure; (c) Long-lasting afterglow degradation in the darkness after the initial light exposure; (d) Recycling stability after different cycles.

Figure 8b shows the formaldehyde degradation curves of the wood materials with CDs/TiO₂@SAO composite coatings under intermittent UV or visible light exposure. The photocatalytic process of formaldehyde was divided into two parts, such as photo degradation (keep lighting for 20 min) and darkness degradation (keep in the dark for 40 min). It can be seen clearly that the photocatalytic response was obviously improved with the additional energy supply (UV or visible light) for the degradation system owing to the good energy storage-release behavior of SAO phosphors. This is consistent with the long-lasting afterglow decay of CDs/TiO₂@SAO composites (Figure 6d). Additionally, the photocatalytic degradation efficiency under UV irradiation was higher than that under visible illumination, which strongly agrees with the variation tendency in the UV-vis diffuse reflectance spectrum of the CDs/TiO₂@SAO composite (Figure 5f).

Owing to the afterglow fluorescence decay and potential photocatalytic activity of the CDs/TiO₂@SAO composite coatings in the darkness, the long-lasting self-luminous degradation of formaldehyde after an initial light exposure was performed to simulate the catalytic activity of wood materials at night when the visible light is turned off (Figure 8c). For comparison, the photocatalytic behaviors of TiO₂ and CDs/TiO₂@SAO composites have also been examined in the same experimental conditions. As shown in Figure 8c, when the external CFL visible excitation light (keep lighting for 60 min) was turned off, the TiO₂ coated wood materials showed negligible photocatalytic activity for the degradation of formaldehyde. However, the functional wood with CDs/TiO₂@SAO composite coatings still maintained photocatalytic activities at a certain level for ~360 min owing to the self-provided light from the SAO self-luminous phosphors. Though the afterglow decay

lifetime of the wood with CDs/TiO₂@SAO composite coatings was obviously more than 6 h (≥ 3.19 mcd/m²), the degradation activity after 180 min seemed negligible owing to the relatively weak inner-lighting of the CDs/TiO₂@SAO photocatalytic system. Figure 8d shows the recycling stability of the functional wood with CDs/TiO₂@SAO composite coatings for the degradation of formaldehyde. The photocatalytic recyclability test under CFL visible illumination was performed in 6 cycles (30-min UV exposure, 8 hours' visible illumination, and 24 h in the darkness before every cycle) and showed that the CDs/TiO₂@SAO composite coatings on wood materials had stable photostability after 6 cycles. These results fully implied that the as-prepared CDs/TiO₂@SAO core-shell catalyst and the coated wood materials with CDs/TiO₂@SAO composite coatings had stable photostability under ambient light sources and a dark environment.

Figure 9 shows the afterglow self-luminous wood materials with CDs/TiO₂@SAO composite coatings compared with the control wood. It was apparent that the composite coating was basically transparent and did not affect the color of the wood surface (Figure 9a), which is necessary for the indoor decorative wood materials. Moreover, as shown in Figure 9e–h, the wood materials with CDs/TiO₂@SAO composite coatings presented long-term afterglow luminescence after suitable light energy storage (UV or visible light), which is consistent with the long-afterglow decay lifetime result of CDs/TiO₂@SAO composites.

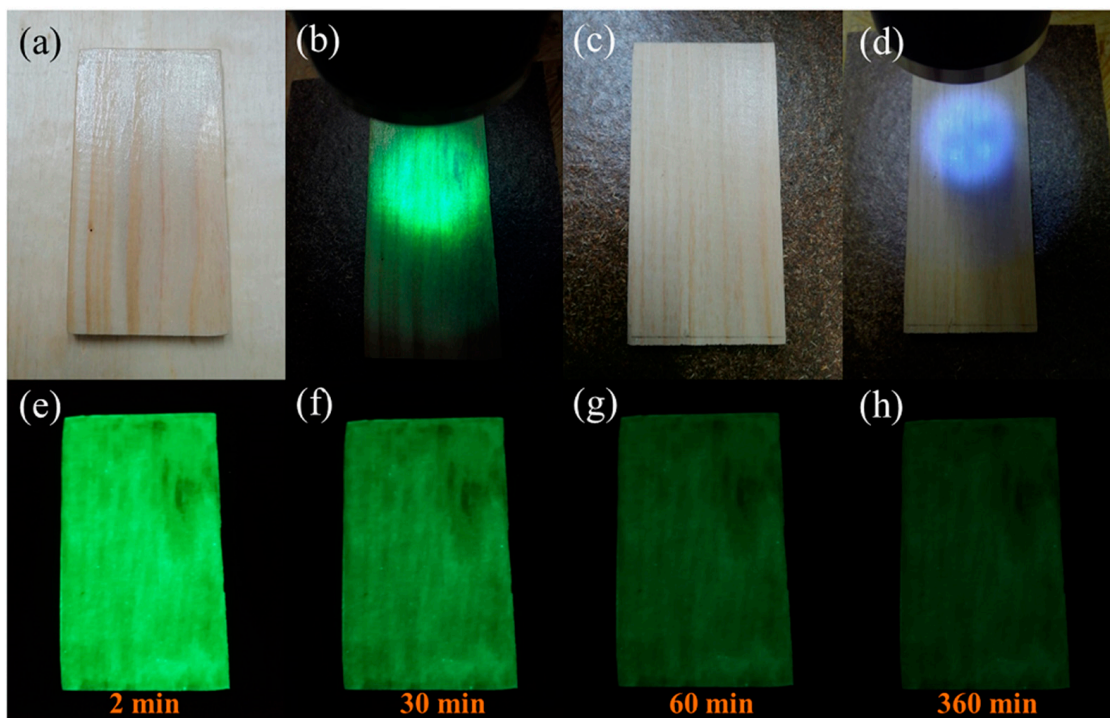


Figure 9. Long-lasting afterglow self-luminous wood materials with CDs/TiO₂@SAO composite coatings compared with the control wood without luminescent coating: Functional wood with CDs/TiO₂@SAO composite coatings (a) under daytime and (b) UV light exposure; Control wood (c) under daytime and (d) UV light exposure; (e–h) Self-luminous behavior of CDs/TiO₂@SAO composite coatings at different lifetimes after the UV light exposure.

The potential photocatalytic mechanism for the CDs/TiO₂@SAO self-luminous photocatalyst in the degradation of formaldehyde pollution was illustrated in Figure 10. For the pristine N,P-doped CDs, with UV light or visible light exposure, the electrons in the valentine band (VB) were partially excited to the conduction band (CB), and some of these excited electrons can react with O₂ directly to produce $\bullet\text{O}_2^-$ radicals for the degradation of formaldehyde [42]. Additionally, the holes (h⁺) can attack the formaldehyde molecule and decompose it into CO₂ and H₂O ultimately. For the CDs/TiO₂@SAO composite photocatalyst, with excitation of a light source (UV or visible light), electron transfers between

tightly bonded N,P-doped CDs and TiO₂ nanoparticles may occur and generate lots of hot electrons [43]. Meanwhile, the SAO long afterglow phosphor can capture and store luminous energy efficiently and give out visible light (green) in a dark environment. When the light excitation source was turned off, the CDs/TiO₂@SAO composites could emit long-lasting luminescence (from strong to weak afterglow brightness) continually at night for a few hours, which could be absorbed and re-utilized by the CDs/TiO₂ composite for photocatalytic degradation of formaldehyde [44,45]. Therefore, owing to the synergistic effect of CDs/TiO₂ nanoparticles and the afterglow luminescence from SAO phosphors, the as-prepared CDs/TiO₂@SAO composite presents a continuous and efficient photocatalytic activity for the degradation of formaldehyde under indoor visible illumination and in a dark environment.

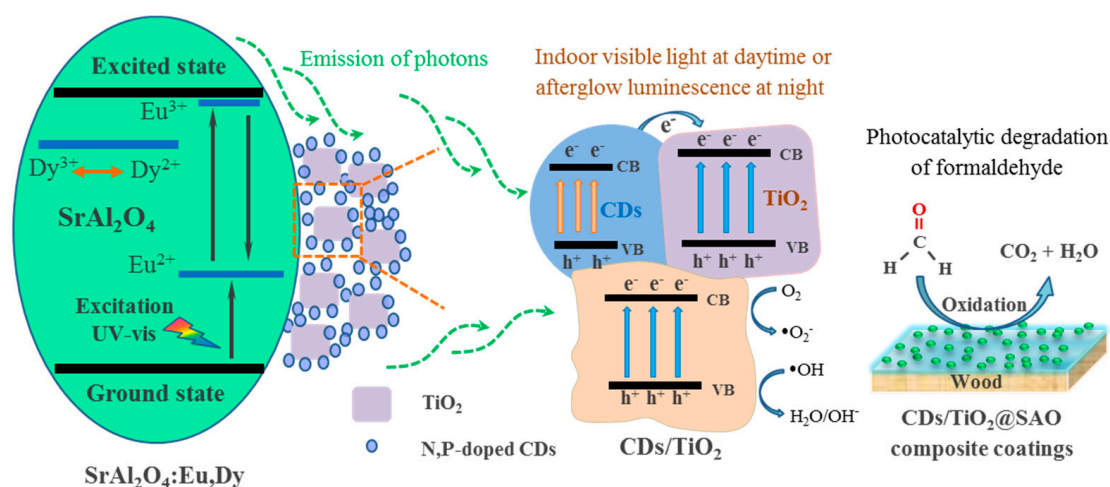


Figure 10. Schematic of the photocatalytic mechanism for the functional wood materials with the long-afterglow self-luminous CDs/TiO₂@SAO composite photocatalyst in the degradation of formaldehyde pollution.

4. Conclusions

In conclusion, a novel efficient self-luminous wood coating with CDs/TiO₂ nano-material coated long afterglow SAO composite (CDs/TiO₂@SAO) was constructed for the photocatalytic degradation of indoor formaldehyde pollution. The photocatalytic degradation reaction of formaldehyde reached ~60% in a 160-min cycle under visible light ($\lambda \geq 400$ nm) owing to the synergistic effect of potential electron transfer between fluorescent CDs and anatase TiO₂ nanoparticles. In addition, owing to the long-lasting luminescence of SAO phosphor at night, the as-prepared CDs/TiO₂@SAO composite photocatalyst can store luminous energy efficiently during the daytime so as to emit visible self-luminescence continuously for a few hours in the absence of light exposure. Furthermore, the wood coating with CDs/TiO₂@SAO composites also maintained a continuous and efficient photocatalytic activity in ~360-min for degrading formaldehyde pollution in the darkness owing to the self-provided visible light from the SAO long-afterglow phosphors. The current research implies that fluorescent CDs and self-luminous SAO-modified traditional anatase TiO₂ catalysts could enhance the photocatalytic activity and achieve long-term photocatalysis for indoor air clean-up in the daytime with an indoor visible light supply and a dark environment without any additional visible light sources.

Author Contributions: Conceptualization, methodology, validation, writing—original draft preparation, composites fabrications, L.Z.; validation, formal analysis, Y.W. and L.P.; supervision, project administration, editing, S.L.; validation, review, editing, Z.C. and S.W. All authors have read and agreed to the published version of the manuscript.

Funding: This research was funded by the National Natural Science Foundation of China (32001261), the basic research funds of central level public welfare research institutes (CAFYBB2022MB001), and the Open Fund Program of the Key Laboratory (2019KFJJ13).

Institutional Review Board Statement: “Not applicable” for studies not involving humans or animals.

Data Availability Statement: The data that allowed for the writing of this article are available for request from the Wood Functional Materials department/Research Institute of Wood Industry/Chinese Academy of Forestry.

Conflicts of Interest: The authors declare no conflict of interest.

References

1. Zhang, X.; Gao, B.; Creamer, A.E.; Cao, C.; Li, Y. Adsorption of VOCs onto engineered carbon materials: A review. *J. Hazard. Mater.* **2017**, *338*, 102–123. [[CrossRef](#)] [[PubMed](#)]
2. Park, J.S.; Ikeda, K. Variations of formaldehyde and VOC levels during 3 years in new and older homes. *Indoor Air* **2006**, *16*, 129–135. [[CrossRef](#)] [[PubMed](#)]
3. Mahmood, A.; Shi, G.; Wang, Z.; Rao, Z.; Xiao, W.; Xie, X.; Sun, J. Carbon quantum dots-TiO₂ nanocomposite as an efficient photocatalyst for the photodegradation of aromatic ring-containing mixed VOCs: An experimental and DFT studies of adsorption and electronic structure of the interface. *J. Hazard. Mater.* **2021**, *401*, 123402. [[CrossRef](#)] [[PubMed](#)]
4. Yu, C.W.; Kim, J.T. Long-term impact of formaldehyde and VOC emissions from wood-based products on indoor environments and issues with recycled products. *Indoor Built Environ.* **2012**, *21*, 137–149. [[CrossRef](#)]
5. Liu, N.; Zhang, X.; Wang, L.; Liang, K.; Zhang, Y.; Cao, J. Early-stage emissions of formaldehyde and volatile organic compounds from building materials: Model development, evaluation, and applications. *Environ. Sci. Technol.* **2022**, *56*, 14680–14689. [[CrossRef](#)]
6. Wolkoff, P.; Nielsen, G.D. Non-cancer effects of formaldehyde and relevance for setting an indoor air guideline. *Environ. Int.* **2010**, *36*, 788–799. [[CrossRef](#)]
7. Liu, L.; Yu, X.; Dong, X.; Wang, Q.; Wang, Y.; Huang, J. The Research on formaldehyde concentration distribution in new decorated residential buildings. *Procedia Eng.* **2017**, *205*, 1535–1541. [[CrossRef](#)]
8. Ogawa, M.; Kabe, I.; Terauchi, Y.; Tanaka, S. A strategy for the reduction of formaldehyde concentration in a hospital pathology laboratory. *J. Occup. Health* **2019**, *61*, 135–142. [[CrossRef](#)]
9. Nielsen, G.D.; Larsen, S.T.; Wolkoff, P. Recent trend in risk assessment of formaldehyde exposures from indoor air. *Arch. Toxicol.* **2013**, *87*, 73–98. [[CrossRef](#)]
10. Bouras, D.; Rasheed, M.; Barille, R.; Aldaraji, M.N. Efficiency of adding DD3+ (Li/Mg) composite to plants and their fibers during the process of filtering solutions of toxic organic dyes. *Opt. Mater.* **2022**, *131*, 112725. [[CrossRef](#)]
11. Wang, W.; Zhang, D.; Ji, Z.; Shao, D.; Sun, P.; Duan, J. High efficiency photocatalytic degradation of indoor formaldehyde with silver-doped ZnO/g-C₃N₄ composite catalyst under the synergistic effect of silver plasma effect and heterojunction. *Opt. Mater.* **2021**, *111*, 110721. [[CrossRef](#)]
12. Shao, Y.; Wang, Y.; Zhao, R.; Chen, J.; Zhang, F.; Linhardt, R.J.; Zhong, W. Biotechnology progress for removal of indoor gaseous formaldehyde. *Appl. Microbiol. Biot.* **2020**, *104*, 3715–3727. [[CrossRef](#)] [[PubMed](#)]
13. Moulis, F.; Krýsa, J. Photocatalytic degradation of several VOCs (n-hexane, n-butyl acetate and toluene) on TiO₂ layer in a closed-loop reactor. *Catal. Today* **2013**, *209*, 153–158. [[CrossRef](#)]
14. Pelaez, M.; Nolan, N.T.; Pillai, S.C.; Seery, M.K.; Falaras, P.; Kontos, A.G.; Dunlop, P.S.M.; Hamilton, J.W.J.; Byrne, J.A.; O’Shea, K.; et al. A review on the visible light active titanium dioxide photocatalysts for environmental applications. *Appl. Catal. B-Environ.* **2012**, *125*, 331–349. [[CrossRef](#)]
15. Luchechko, A.; Zhydachevskyy, Y.; Ubizskii, S.; Kravets, O.; Popov, A.I.; Rogulis, U.; Elsts, E.; Bulur, E.; Suchocki, A. Afterglow, TL and OSL properties of Mn²⁺-doped ZnGa₂O₄ phosphor. *Sci. Rep.* **2019**, *9*, 9544. [[CrossRef](#)]
16. Li, J.; Ren, D.; Wu, Z.; Xu, J.; Bao, Y.; He, S.; Chen, Y. Flame retardant and visible light-activated Fe-doped TiO₂ thin films anchored to wood surfaces for the photocatalytic degradation of gaseous formaldehyde. *J. Colloid Interf. Sci.* **2018**, *530*, 78–87. [[CrossRef](#)]
17. Etacheri, V.; Seery, M.K.; Hinder, S.J.; Pillai, S.C. Highly visible light active TiO_{2-x}N_x heterojunction photocatalysts. *Chem. Mater.* **2010**, *22*, 3843–3853. [[CrossRef](#)]
18. Ferrighi, L.; Datto, M.; Fazio, G.; Di Valentin, C. Catalysis under cover: Enhanced reactivity at the interface between (doped) graphene and anatase TiO₂. *J. Am. Chem. Soc.* **2016**, *138*, 7365–7376. [[CrossRef](#)]
19. Gan, J.; Wu, Y.; Yang, F.; Zhang, H.; Wu, X.; Wang, Y.; Xu, R. Wood-cellulose photoluminescence material based on carbon quantum dot for light conversion. *Carbohydr. Polym.* **2022**, *290*, 119429. [[CrossRef](#)]
20. Zhang, L.; Lyu, S.; Zhang, Q.; Chmely, S.C.; Wu, Y.; Melcher, C.; Rajan, K.; Harper, D.P.; Wang, S.; Chen, Z. Recycling hot-water extractions of lignocellulosic biomass in bio-refinery for synthesis of carbon nanoparticles with amplified luminescence and its application in temperature sensing. *Ind. Crops Prod.* **2020**, *145*, 112066. [[CrossRef](#)]

21. Zhang, L.; Lyu, S.; Zhang, Q.; Wu, Y.; Melcher, C.; Chmely, S.C.; Chen, Z.; Wang, S. Dual-emitting film with cellulose nanocrystal-assisted carbon dots grafted SrAl₂O₄:Eu²⁺,Dy³⁺ phosphors for temperature sensing. *Carbohydr. Polym.* **2019**, *206*, 767–777. [[CrossRef](#)] [[PubMed](#)]
22. Jing, S.; Zhao, Y.; Sun, R.C.; Zhong, L.; Peng, X. Facile and high-yield synthesis of carbon quantum dots from biomass-derived carbons at mild condition. *ACS Sustain. Chem. Eng.* **2019**, *7*, 7833–7843. [[CrossRef](#)]
23. Di, J.; Xia, J.; Ji, M.; Wang, B.; Yin, S.; Zhang, Q.; Chen, Z.; Li, H. Carbon quantum dots modified BiOCl ultrathin nanosheets with enhanced molecular oxygen activation ability for broad spectrum photocatalytic properties and mechanism insight. *ACS Appl. Mater. Inter.* **2015**, *7*, 20111–20123. [[CrossRef](#)] [[PubMed](#)]
24. Gao, Q.; Yuan, Z.; Yang, G.; Tian, Z.; Jiang, Z.; Zhang, K.; Wang, C.; Chen, J. Enhancement of lignin-based carbon quantum dots from poplar pre-hydrolysis liquor on photocatalytic CO₂ reduction via TiO₂ nanosheets. *Ind. Crops Prod.* **2021**, *160*, 113161. [[CrossRef](#)]
25. Martins, N.C.; Ângelo, J.; Girão, A.V.; Trindade, T.; Andrade, L.; Mendes, A. N-doped carbon quantum dots/TiO₂ composite with improved photocatalytic activity. *Appl. Catal. B-Environ.* **2016**, *193*, 67–74. [[CrossRef](#)]
26. Hu, Y.; Xie, X.; Wang, X.; Wang, Y.; Zeng, Y.; Pui, D.Y.; Sun, J. Visible-light upconversion carbon quantum dots decorated TiO₂ for the photodegradation of flowing gaseous acetaldehyde. *Appl. Surf. Sci.* **2018**, *440*, 266–274. [[CrossRef](#)]
27. Zhang, L.; Lyu, S.; Chen, Z.; Wang, S. Preparation and characterization of dual-functional coatings of nanofibrillated cellulose and modified SrAl₂O₄: Eu, Dy phosphors. *Surf. Coat. Technol.* **2018**, *349*, 318–327. [[CrossRef](#)]
28. Poulouse, A.M.; Anis, A.; Shaikh, H.; Alhamidi, A.; Siva Kumar, N.; Elnour, A.Y.; Al-Zahrani, S.M. Strontium aluminate-based long afterglow PP composites: Phosphorescence, thermal, and mechanical characteristics. *Polymers* **2021**, *13*, 1373. [[CrossRef](#)]
29. Liu, X.; Chen, X.; Li, Y.; Wu, B.; Luo, X.; Ouyang, S.; Luo, S.; Kheraif, A.A.; Lin, J. A g-C₃N₄@Au@SrAl₂O₄:Eu²⁺,Dy³⁺ composite as an efficient plasmonic photocatalyst for round-the-clock environmental purification and hydrogen evolution. *J. Mater. Chem.* **2019**, *7*, 19173–19186. [[CrossRef](#)]
30. Sikandar, M.A.; Ahmad, W.; Khan, M.H.; Ali, F.; Waseem, M. Effect of water resistant SiO₂ coated SrAl₂O₄: Eu²⁺ Dy³⁺ persistent luminescence phosphor on the properties of Portland cement pastes. *Constr. Build. Mater.* **2019**, *228*, 116823. [[CrossRef](#)]
31. Brik, M.G.; Ma, C.G.; Yamamoto, T.; Piasecki, M.; Popov, A.I. First-principles methods as a powerful tool for fundamental and applied research in the field of optical materials. In *Phosphor Handbook*; CRC Press: Boca Raton, FL, USA, 2022; pp. 1–25.
32. Zhang, L.; Lyu, S.; Chen, Z.; Wang, S. Fabrication flexible and luminescent nanofibrillated cellulose films with modified SrAl₂O₄: Eu, Dy phosphors via nanoscale silica and aminosilane. *Nanomaterials* **2018**, *8*, 352. [[CrossRef](#)] [[PubMed](#)]
33. Zhang, R.; Liu, Y.; Yu, L.; Li, Z.; Sun, S. Preparation of high-quality biocompatible carbon dots by extraction with new thoughts on the luminescence mechanisms. *Nanotechnology* **2013**, *24*, 225601. [[CrossRef](#)] [[PubMed](#)]
34. Guo, Y.; Cao, F.; Li, Y. Solid phase synthesis of nitrogen and phosphor co-doped carbon quantum dots for sensing Fe³⁺ and the enhanced photocatalytic degradation of dyes. *Sensor. Actuat. B-Chem.* **2018**, *255*, 1105–1111. [[CrossRef](#)]
35. Gao, L.; Gan, W.; Xiao, S.; Zhan, X.; Li, J. A robust superhydrophobic antibacterial Ag–TiO₂ composite film immobilized on wood substrate for photodegradation of phenol under visible-light illumination. *Ceram. Int.* **2016**, *42*, 2170–2179. [[CrossRef](#)]
36. Sahu, S.; Behera, B.; Maiti, T.K.; Mohapatra, S. Simple one-step synthesis of highly luminescent carbon dots from orange juice: Application as excellent bio-imaging agents. *Chem. Commun.* **2012**, *48*, 8835–8837. [[CrossRef](#)] [[PubMed](#)]
37. Yang, X.; Zhang, Y.; Liu, W.; Gao, J.; Zheng, Y. Confined synthesis of phosphorus, nitrogen co-doped carbon dots with green luminescence and anion recognition performance. *Polyhedron* **2019**, *171*, 389–395. [[CrossRef](#)]
38. Sanzone, G.; Zimbone, M.; Cacciato, G.; Ruffino, F.; Carles, R.; Privitera, V.; Grimaldi, M.G. Ag/TiO₂ nanocomposite for visible light-driven photocatalysis. *Superlattices Microstruct.* **2018**, *123*, 394–402. [[CrossRef](#)]
39. Rojas-Hernandez, R.E.; Rubio-Marcos, F.; Rodriguez, M.Á.; Fernandez, J.F. Long lasting phosphors: SrAl₂O₄: Eu, Dy as the most studied material. *Renew. Sustain. Energy Rev.* **2018**, *81*, 2759–2770. [[CrossRef](#)]
40. Mavengere, S.; Kim, J.S. Photocatalytic properties of g-C₃N₄-supported on the SrAl₂O₄: Eu, Dy/SiO₂. *Coatings* **2020**, *10*, 917. [[CrossRef](#)]
41. Liu, K.; Kong, F.; Zhu, C.; Jiang, G. Photocatalytic activity of phosphorus and nitrogen co-doped carbon quantum dots/TiO₂ nanosheets. *Nano* **2020**, *15*, 2050151. [[CrossRef](#)]
42. Li, N.; Liu, Z.; Liu, M.; Xue, C.; Chang, Q.; Wang, H.; Li, Y.; Song, Z.; Hu, S. Facile synthesis of carbon dots@2D MoS₂ heterostructure with enhanced photocatalytic properties. *Inorg. Chem.* **2019**, *58*, 5746–5752. [[CrossRef](#)] [[PubMed](#)]
43. Chen, Q.; Lin, G.; Meng, L.; Zhou, L.; Hu, L.; Nong, J.; Li, Y.; Wang, J.; Hu, K.; Yu, Q. Enhanced photoelectric performance of TiO₂ nanotubes sensitized with carbon dots derived from bagasse. *Chem. Phys. Lett.* **2020**, *749*, 137428. [[CrossRef](#)]
44. Garcia, C.R.; Oliva, J.; Arroyo, A.; Garcia-Lobato, M.A.; Gomez-Solis, C.; Torres, L.D. Photocatalytic activity of bismuth doped SrAl₂O₄ ceramic powders. *J. Photochem. Photobiol. A* **2018**, *351*, 245–252. [[CrossRef](#)]
45. Zargoosh, K.; Aliabadi, H.M. SrAl₂O₄: Eu²⁺: Dy³⁺/WO₃/polyester nanocomposite as a highly efficient and environmentally friendly photocatalyst for removal of dyes from industrial wastes. *Environ. Nanotechnol. Monit. Manag.* **2019**, *12*, 100273. [[CrossRef](#)]

Disclaimer/Publisher’s Note: The statements, opinions and data contained in all publications are solely those of the individual author(s) and contributor(s) and not of MDPI and/or the editor(s). MDPI and/or the editor(s) disclaim responsibility for any injury to people or property resulting from any ideas, methods, instructions or products referred to in the content.